Chapter 2

Observational Details

The Pulsar Timing Observations reported here were started in July 1995 using the Ooty Radio Telescope (ORT) located in Southern India at a longitude of 76° 40' E, latitude of 11° 22' $56''$, and at an altitude of 2150 metres above sea level. Timing observations were carried out at, regular intervals of approximately one month separation for a year, with one more session in January 1997. This provides us a data set spanning over one and a half pars. A digital signal preprocessor which was built primarily for pulsar search with ORT and GMRT (Giant Metre-wave Radio Telescope) was used as the **backend** with its data recording system. We built a time-stamping unit to record the start time of the observation to an accuracy of $0.1\mu s$. It also measures the drift of the Astronomical Clock (run by the 1 MHz clock referenced to a Rb frequency standard) with respect to the 1 PPS signal from the GPS receiver.

2.1 The Ooty Radio Telescope

2.1.1 Front end of the Telescope

The Ooty Radio Telescope is a linear phased array consisting of 1056 dipoles, grouped into "modules" with 48 dipoles per module, kept at the focus of an off-axis parabolic reflector (Swarup et al 1971, Sarma et al. 1975a, 1975b, Kapahi et al. 1975). The parabolic reflector is 530m long in the north-south direction and 30m wide in the east-west direction and is made of 1100 stainless steel wires running along the north-south direction. The telescope operates at a fixed centre frequency of 326.5 MHz with a bandwidth of 15 MHz and is sensitive to a single polarization oriented along North-South direction. The telescope is on a hill with a slope of 11°, which is equal to the latitude of the place, thus making it an equatorially mounted telescope. A source at zenith can be tracked for about 9 hours (-4 to $+5$ hrs of Hour Angle) by rotating the telescope in the east-west direction. The declination coverage is achieved by phasing the array electronically and is limited to $\pm 55^\circ$.

Fig 2.1 shows the block diagram of a module of the Ooty Radio Telescope. The output from each dipole is passed through a low-noise amplifier and a phase shifter and 48 such

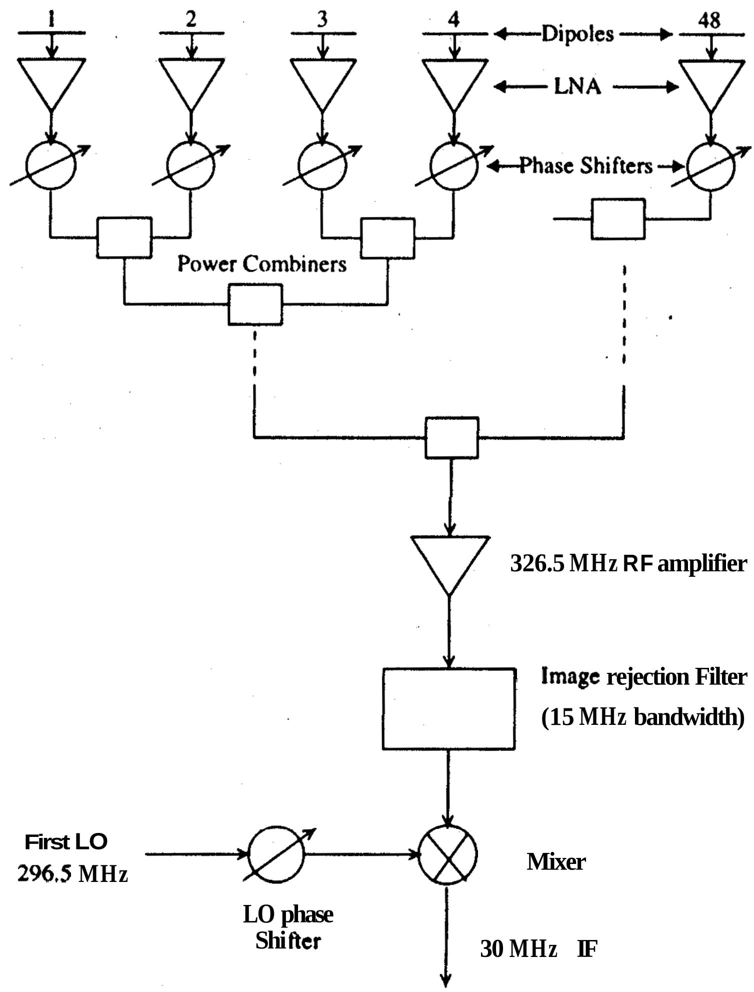

Figure 2.1: Block diagram of a module of the ORT. The abbreviations LNA, RF, IF , and LO represents low noise amplifier, radio frequency, intermediate frequency and Local Oscillator respectively.

dipoles are combined in a Christmas-tree fashion to get one "module". The phase shifter compensates the phase for the centre frequency towards a specified declination within one module. There are 22 such modules which are labelled North 1 to 11 & South 1 to 11 for convenience. The signal from each module is down converted to 30 MHz IF (intermediate frequency) by mixing with a Local Oscillator at a frequency of 296.5 MHz, after passing through an RF amplifier and an image rejection filter of 15 MHz bandwidth. The signal is then brought to the receiver room.

The rest of the front-end electronics of the telescope is kept in the receiver room. The delays due to the path differences between the modules are compensated by adding or taking out cables from the signal path (see fig 2.2). Since the delay compensation is done at 30 MHz, a net phase difference remains which can be compensated in the local oscillator path. The IF signal is amplified by preamplifiers (PA1 & PA2) before and after the delay compensation. The delay compensated signal from each module is then divided using a 12-way power splitter. The 12 sets of outputs from the 11 modules of the North side are combined with different phase gradients by the beam forming network to generate 12 beams around the specified direction. Similarly 12 beams are produced from the 11 modules of the southern half. The 12 north and south beams are then either added or correlated to get a total power or correlation beam respectively. The correlation and total power beams have width of $3.3\sec(\delta)$ arcmin and $5.5\sec(\delta)$ arcmin respectively in the north-south direction and both the beams have a width of 2° in the east-west direction. The 12 beams span $\pm 18'$ around the specified declination with a separation $3\sec(\delta)$ arcmin. For pulsar timing observations, we have used the central total power beam (Beam 7).

2.1.2 System Temperature and Sensitivity of the Telescope

The power in a radio receiver is usually expressed as a noise temperature T being equal to the amount of noise power picked up by a dipole when immersed in a black-body of temperature T. The minimum detectable change in temperature or sensitivity of the telescope is given by

$$\Delta T_{\rm min} = \frac{\eta T_{\rm sys}}{\sqrt{\Delta f\, t}} \tag{2.1}$$

where η is the signal-to-noise ratio desired, $T_{\rm sys}$ is the system noise temperature, Δf is the pre-detection bandwidth and t is the total integration time (in secs). The system temperature is the sum of the receiver noise temperature, the system temperature due to sky noise from diffuse background and other radio sources and a contribution from the ground pick up due to the 'spill-over'. In a radio receiver the 'receiver noise' is contributed by the local electronics - amplifiers, mixers, detectors, attenuators and other components. The degradation of signal-to-noise ratio due to attenuation in the signal path can be improved by amplifying the signal before the path which introduces attenuation. The amplifier noise can be reduced by employing low-noise amplifiers (LNA) to boost the signal. The ORT was upgraded in 1992 by introducing LNAs in the front-end. The system temperature can be computed by considering a model of the receiver system to obtain $T_{\rm rec}$

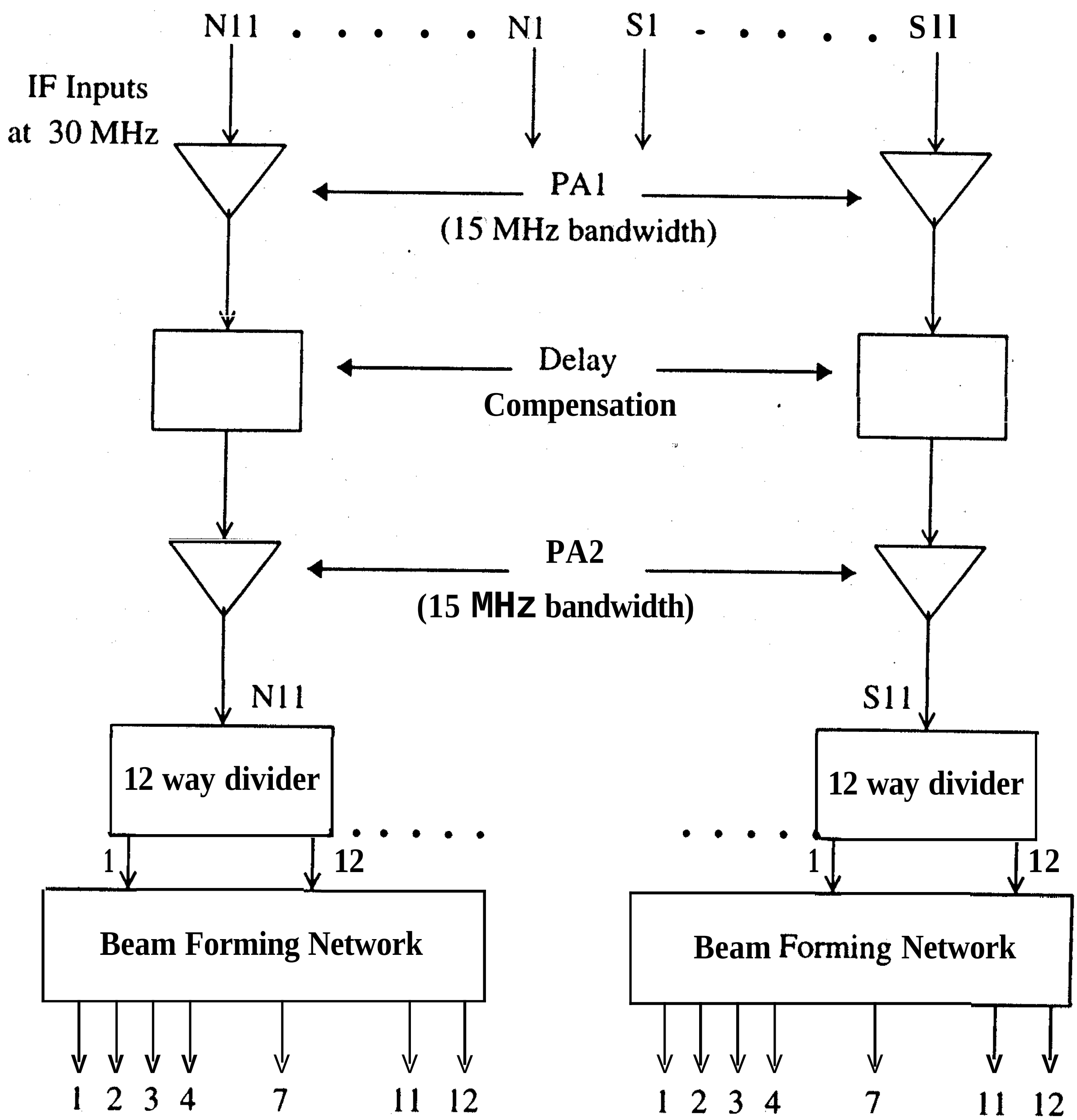

Figure 2.2: Block diagram of the Front End of the ORT. N & S stand for North and South halves of the telescope, numbers next to N & S are module numbers, PA1 and PA2 are preamplifiers and the numbers 1 to 12 below the beam forming network are the 12 beams having a separation of 6' between them in the North-South direction.

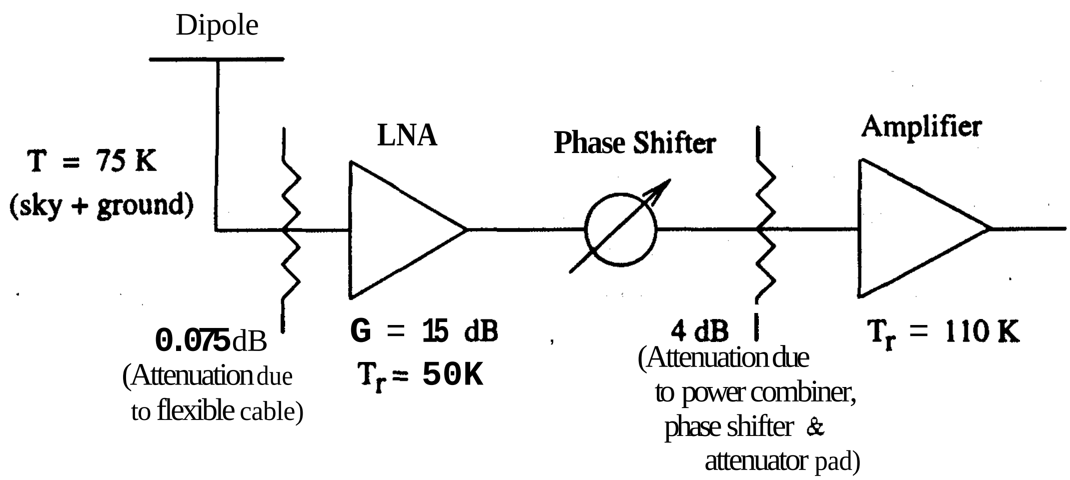

Figure 2.3: A model of the ORT receiver system for system **temperature** computation

---

and then adding the contribution due to the ground T_{gr} and the sky **background** T_{sky}. Computed values for T_{sky} and T_{gr} for the ORT are 45 **K(typical)** and 30 K, respectively.

The model for the receiver system is shown in fig(2.3). The dipole output is **connected** to the low-noise amplifier using a flexible cable which has an attenuation of 0.075 dB. The input equivalent noise temperature of the **LNA** is 50 K and its gain is 15 dB. The phase shifters, the power combiners (combining the signal from 48 dipoles) and the **attenuator** pad together have a total attenuation of 4 dB. The signal is then amplified using an amplifier of noise temperature 110 K. The noise contribution **from** successive stages can be neglected since they are weighted down by the gain of the previous stages. Hence the receiver temperature can be written as

$$T_{rec} = T_{amb}\frac{(1-\alpha_1)}{\alpha_1} + \frac{T_{amp1}}{\alpha_1} + T_{amb}\frac{(1-\alpha_2)}{\alpha_1\alpha_2 G} + \frac{T_{amp2}}{\alpha_1\alpha_2 G} \tag{2.2}$$

where T_{amb} is the ambient temperature (295 K), T_{amp1} & T_{amp2} are the noise temperatures (50 K & 110 K) of the two amplifiers respectively, α_1(0.983) & α_2(0.398) are the fraction of input power available at the other end of the attenuator. The total system temperature is –150 K (Anish **Roshi**,1996) after adding the T_{sky} and T_{gr} to T_{rec}.

The signal from an astronomical source is also noise like. **The** presence of the source is reflected in an enhancement of the noise power by T_A, called the 'Antenna Temperature'. For an unresolved source the antenna temperature is proportional to the source **flux** and is related to it by

$$SA_{eff} = k_B T_A \tag{2.3}$$

where k_B is the **Boltzmann** constant and A_{eff} is the effective aperture area. .

The conventional way of measuring the sensitivity for the ORT is to determine the signal-to-noise ratio of a 1 Jy (1 Jy = 10^{-26} W Hz^{-1} m^{-2}) source using the correlated beam (beam 7) with a bandwidth of 4 **MHz** and integration time of 1 second. This is measured by pointing the telescope towards a calibrator source and determining the increase in output power with respect to an off-source position. The ratio of the increase in power to the r.m.s of the off-source signal fluctuations gives the signal-to-noise ratio. The fluctuations in the off-source position are due to amplifier noise (mainly RF amplifiers), the noise picked up from the ground due to 'spill-over' and the noise due to the background radiation from the sky. The signal-to-noise ratio measured on a 1 Jy source for ORT, on an average, is $\sim$ 25. With this sensitivity, the minimum flux density of the pulsar detectable with S/N of 10 is $\sim$ 2 mJy with 8 MHz bandwidth and integration done over 10 minutes.

2.2 The Pulsar Receiver

The pulsar receiver that we used was built mainly for the purpose of pulsar search (Ramkumar et al. 1994). The schematic diagram of the pulsar receiver is shown in fig(2.4). The North and South signals from beam-7 are combined and down converted to baseband using a second Local Oscillator at a frequency of 33.5 MHz, with a power level of +7 dBm.

2.2.1 Pulsar Search Pre-processor

The front end of the pulsar receiver consists of a 4-bit sampler (A/D converters), which samples the incoming baseband signals of 8 MHz at the Nyquist rate and feeds them into a 512-point FFT engine. This FFT engine produces 256-point complex spectra which are converted to power spectra using look-up tables. The resultant power spectra are pre-integrated over successive spans of $\sim$0.5 msec defining our sampling interval. A block integration is done over a programmable number of pre-integrated samples (16 to 256 samples) for calculation of the running mean for each of the 256 frequency channels. Before the next block-integrated data is ready, the control PC computes the running mean over a prc-specified time (0.5 secs to 4 minutes, we have chosen $\sim$ 4 secs) and supplies these values to a mean subtractor which removes the mean from the pre-integrated data stream. The same PC also computes scale factors to equalize the gains of the spectral channels (only when the output is 2 or more bits per sample) in the pass band and supplies them so that it can be used as a gain calibration look-up table for correcting the bandshape of the mean subtracted data. In one-bit mode of operation, gain calibration scale factors are set to unity for all channels. In our case, the mean subtracted values are one-bit quantized and stored on magnetic tapes. With a sampling interval of 0.5 msec, roughly one million one-bit samples per frequency channel are collected in 10 minutes of observation.

2.2.2 Routine check of the observational set-up

During every observing session, a strong continuum source was observed to simulate a pulsar signal (with DM=0) at the front end of the receiver for checking the observational set-up before starting the regular observations (see fig 2.5). The beam-7 North signal was passed through a phase switch inverting circuitry, which introduces a $0°$ or $180°$ phase

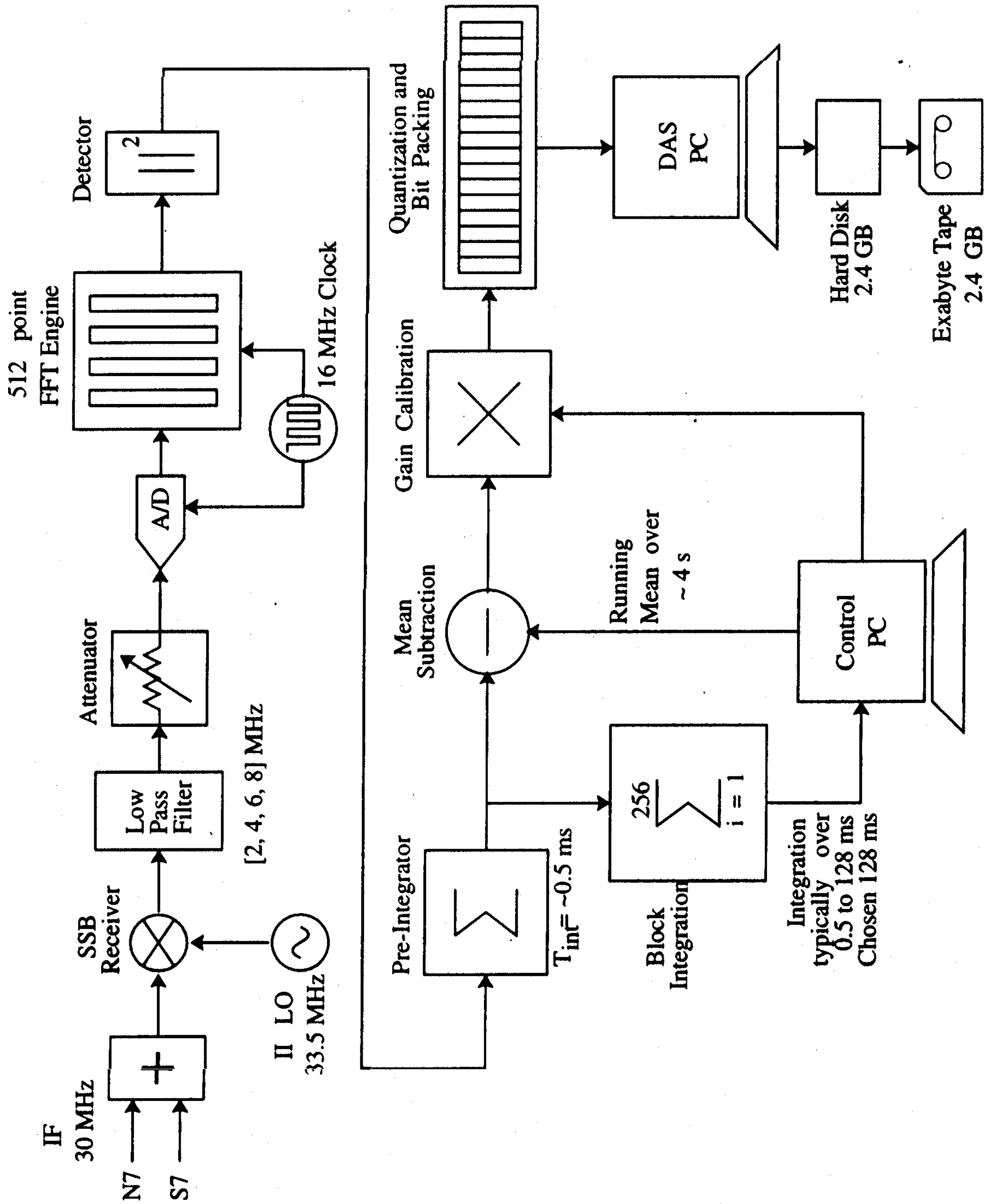

Figure 2.4: Schematic diagram of the Pulsar Receiver System. SSB receiver represents the Single Sideband Receiver.

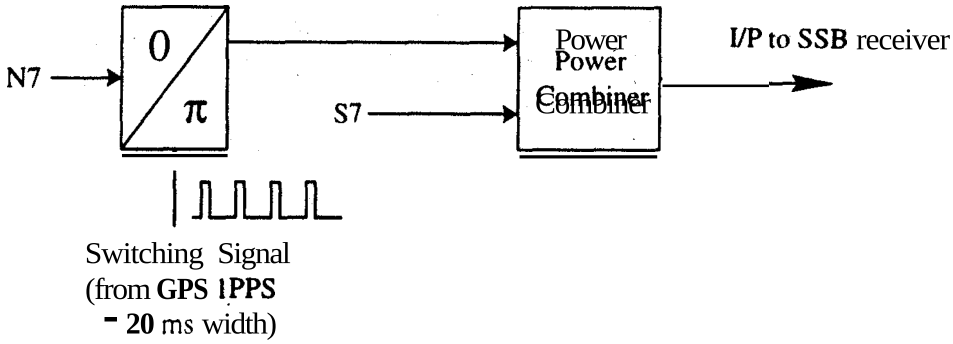

Figure 2.5: Set-up used to simulate pulsar from a continuum source

shift in tile signal path when the switching signal is low or high respectively. The switched North signal was then added to the South signal to obtain an effective beam switching mode. A switching signal of 1 PPS (1 pulse per second) rate, obtained from the GPS receiver was used for this purpose. This set-up produces a pulsar like signal (with a pulse width of 20 msec and a period of 1 sec) at the input of the pulsar receiver, such that the peak flux density in the pulse is equal to the continuum source flux. Like any other pulsar, this simulated pulsar is also observed for 10 minutes. Mainly these observations were used to determine the variations in the clock frequency of the sampler. This is essential because the clock frequency is produced by a free-running crystal which is not tied up with any local frequency standard and it shows variations of the order of 5–10 parts in million over timescales of months. These variations were then corrected during the analysis. These observations can also be used to calibrate the flux of the pulsed emission by knowing the flux of the calibrator source and the running mean (for details see Ramkumar et al. 1994). We have riot pursued this calculation in our current study.

2.3 Time Stamping Set-up

Although the prototype of the pulsar search pre-processor was available at ORT, accurate time measurement was not possible with the existing system. We have therefore built a time-stamping unit for our timing observations (fig 2.6). An Astronomical clock run on a Rb frequency standard was used to read the start time of the observations in terms of the Indian Standard Time (IST = Universal Time + 5.5hrs). The Rb standard is monitored for any frequency drift using an GPS receiver making use of the 1 PPS signal from it. The time stamping unit compares the 1 PPS signal from the GPS receiver and the 1 PPS from the Astronomical clock and displays the time difference (Δt_A) between the two to an accuracy of $0.1\mu s$. The jitter in the 1 PPS signal from the GPS receiver is of the order of ± 300ns. Hence, Δt_A at any time also will have the same amount of jitter in it. However, with suitably long term monitoring, one would be able to estimate the generally slow drift to a better accuracy. We therefore do not use the GPS receiver directly to drive the Astronomical clock. The Rb frequency standard is employed for the purpose. This also allowed us the choice to switch the **GPS** unit off during observations so as to avoid possible radio-frequency interference from it, provided we sampled the clock drift often enough as a part of the long term monitoring. In the beginning of every observing session, the clock was adjusted in such a way that Δt_A goes to zero. The amount of accumulated drift seen in a day is typically $\sim +4\mu s$. The time stamping unit also found the time difference, Δt_B, between the acquisition start pulse (coming from the pulsar receiver) and the following end of second to an accuracy of $0.1\mu s$ whenever the acquisition starts. The Start IST noted at the start of each acquisition with the completed integral seconds is stored in a register. So, T_{start}, the actual start time of the observation is determined as follows.

$$T_{start} = \text{Start IST} + \Delta t_A - \Delta t_B \tag{2.4}$$

At the end of the every 10 minute run, stored values of the start IST (hh:mm:ss), Δt_A and Δt_B are passed from the 'Time stamping unit' to the control PC, where this information is logged in a (tstamp) file sequentially.

2.4 Source selection criteria and observational strategy

We selected $\sim$ 30 recently discovered southern pulsars whose period derivatives (P) were yet to be determined. These pulsars are chosen to meet the criterion that they lie within $\pm 55°$ declination zone, considering the reduction in the sensitivity of ORT at higher declinations. Also, it was ensured that they are detectable in 10 minutes of integration with a signal-to-noise ratio ≥ 50, using the following equation

$$S_{min} = \frac{\eta}{G} \frac{T_{sys}}{\sqrt{N_{pol}\Delta f \tau}} \left(\frac{W}{P-W}\right)^{1/2} \tag{2.5}$$

where S_{min} is the minimum detectable flux, η is the required signal-to-noise ratio, G is the ratio of effective aperture area to twice the Boltzmann constant (i.e. $A_{eff}/2k_B$), N_{pol} is the number of polarisation (=1 in the present case), Af is the total bandwidth used, τ is the integration time, W is the width of the pulse and P is the period of the pulsar. However, given the available observing time, in the first go, we have attempted long term monitoring of only 16 pulsars. Along with this set of pulsars, the pulsar **J1735-0724** whose P is known was also observed to allow thorough testing of our observational and analysis procedure.

In the beginning of every observing session a strong pulsar was observed and analysed immediately to ensure that the observational set-up was in a good condition. Every pulsar was observed for 10 minutes twice a day on atleast two days every month. So far, the observations have been carried out for 1 year continuously from July 1995 to July 1996, and one more set of observations was obtained after a gap of six months. But in the first observing session we observed every pulsar for 10 minutes each with few tens of minutes of separation and then with a few hours of separation and then with a day separation (this is for reasons which will be clear in the chapter 3). Every day during the observing

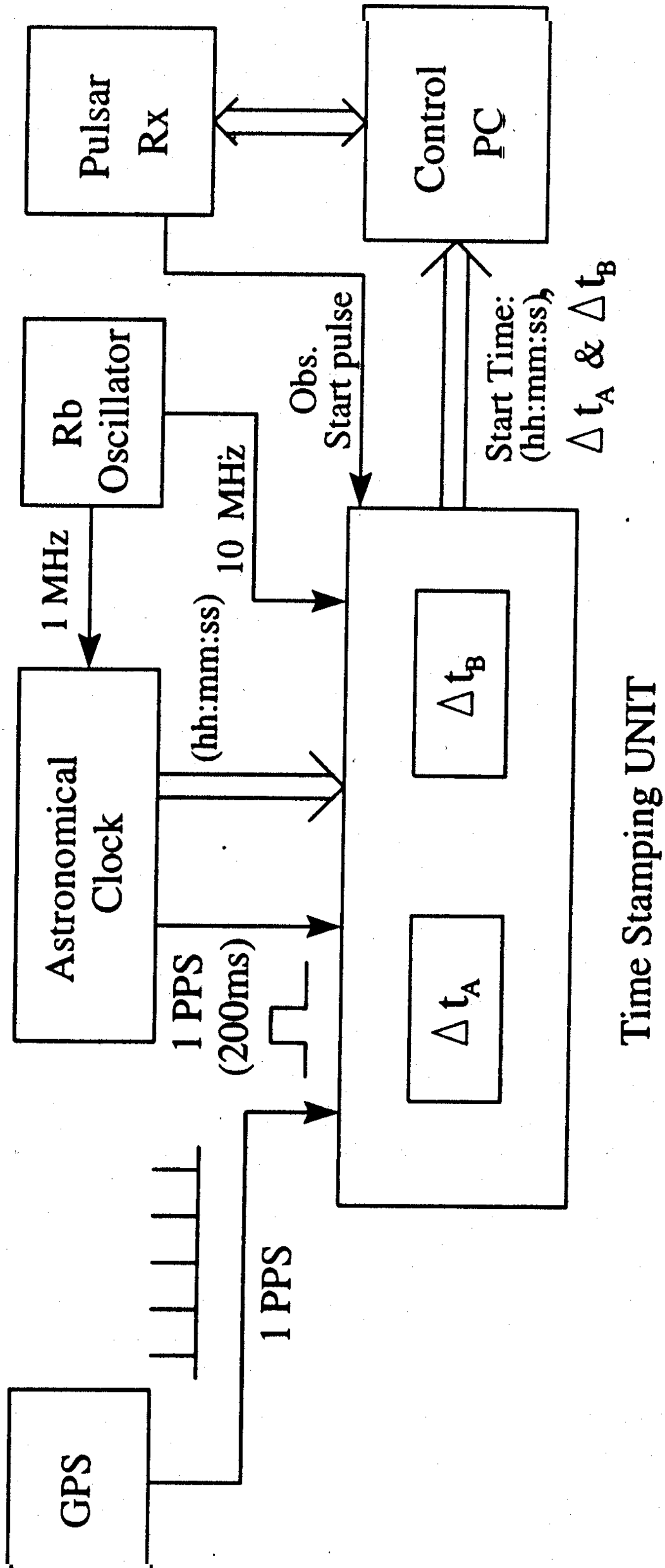

Figure 2.6: Time Stamping Set-up

session a strong continuum source was observed as explained in section 2.2.2 to calibrate the backend receiver as well as to determine the variations in the clock frequency of the sampler. The clock variations were then corrected during analysis.

2.5 Problems faced during observations

One of the main problems faced during the observations was the interference due to sprayers used by farmers in the nearby fields during daytime and that due to bad TV boosters during evenings. So whenever the interference was not broadband, we noted the affected channel numbers because of this by looking at the online display of the average spectrum and later on we removed those channels from our analysis. Observations also suffered from some local problems like frequent power failures and heavy winds especially during rainy seasons. Occasionally the GPS receiver would track less than 4 satellites, while 4 is the minimum number required to maintain the accuracy of the 1 PPS pulse to within ±300 ns.

Summary of this chapter

- We describe the observational set-up implemented with the Ooty Radio Telescope and the timing obervations of 16 pulsars carried out with this system.
- The details of the telescope and the pulsar receiver are described in this chapter.
- We describe the time-stamping set-up built to note the starting time of the observation to an accuracy of $0.1\mu s$ using a GPS receiver and also to monitor the drift of the Astronomical Clock which is run by a Rb frequency standard with respect to the GPS time.
- We have also discussed the sample selection, the observing procedure and the problems we faced during our observations.

Chapter 3

Timing Analysis Procedure

Pulsar Timing Analysis consists of a series of stages: first determining the arrival time of the pulse at the observatory; then translating these local arrival times to the arrival times at the Solar System Barycentre by removing Earth's motion, dispersive delay at the centre frequency and other relativistic effects. Rotational and Positional parameters of a pulsar can be obtained by comparing the barycentric arrival times of the pulses with the expected arrival times baaed on timing models of pulsar rotation. Our timing analysis were performed off-line in such a series of stages.

3.1 Measurement of Local Arrival Times of pulses

The primary data recorded is a series of sample frames separated by —0.5 **msec** in time with each frame consisting of **256** one-bit values corresponding to the **256** frequency channels in each sample. Each observing run is normally $\sim$9 minutes long, giving a single file of size $\sim$34 Megabytes.

The pulsar signal gets dispersed due to the free electrons in the intervening medium and hence the signal at a lower frequency arrives later in comparison to the signal at a higher frequency (fig 3.1). This causes a smearing of the pulse when observed over a finite

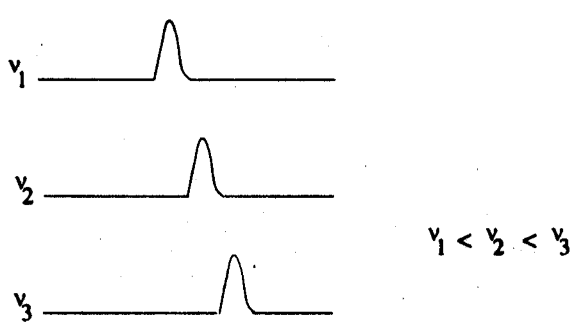

Figure 3.1: Dispersive delay at lower frequencies

bandwidth, resulting in a reduction in peak flux and hence the signal-to-noise ratio. The time smearing that results from a given bandwidth $\Delta\nu$ at a centre frequency ν_0 for a given column density of electrons, defined as dispersion measure (DM), is

$$\Delta t \simeq 8.3\mu s \frac{\mathrm{DM(pc\ cm^{-3})}\Delta\nu(\mathrm{MHz})}{\nu_0^3(\mathrm{GHz})} \tag{3.1}$$

where $\Delta\nu << \nu_o$. The bandwidth can be reduced to limit dispersion, but this reduces the sensitivity. To overcome this problem one can use many narrow frequency channels within the wide band available. In the post-detection analysis, the relative dispersion between these channels can be removed by applying appropriate delays to individual channels with respect to a reference frequency which is generally the centre frequency of observation. This is known as 'incoherent dedispersion' because the signals are combined after detection. In our case, the spectral channel width of 31.25 KHz (256 channels across 8 MHz bandwidth) results in a smearing of 0.5 msec (equal to our sampling interval) for a dispersion measure of $\approx$ 70 pc $\mathrm{cm^{-3}}$. First, we dedisperse the data by correcting for the delay gradient across the channels and then average the channel contributions corresponding to each of the 0.5 msec samples.

In this process of incoherent de-dispersion, the dispersion delay within each of the spectral channels, however, remains uncorrected. At high dispersion measures and at low frequencies, such uncorrected dispersion delay may still dominate the pulse width. Although this smearing could be reduced by reducing the width '$\Delta\nu$' of individual frequency channels further, the effective time-resolution would be limited to $\Delta t = \frac{1}{\Delta\nu}$, since independent samples are available only at time intervals of $1/\Delta\nu$. Therefore for a given observing frequency and DM, there exists an optimum channel width below which the sampling limit prevails and above which the dispersion smearing dominates. At frequency of 327 MHz the best time resolution possible is $\sim 30\mu s$ at low DMs, and at a DM of $\sim$100 the best achievable time resolution rises to $\sim 100\mu s$. In the present case, however, given the sampling interval of 0.5 msec, and the intrinsic pulse widths of pulsars in our sample are likely to be of the order of a few msec, the dispersion smearing within the spectral channels for even DMs as high as 250 may be tolerable.

After de-dispersion, the resultant time series were 'folded' synchronous with an apparent period predicted on the basis of previous estimates of the pulsar parameters and the ephemeris of the Earth's motion. The folding was performed by computing the pulse phase for each sample with respect to the first sample and adding the sample in the correct pulse phase 'bin'. A counter was set to keep track of the additions in each bin for subsequent normalisation. In the present case the number of phase bins used for folding was kept 10 times larger than that required in the final average. A given sample was added to the finer bin corresponding to the phase nearest to the sample phase. At the end the resultant profile was produced by bunching the finer bins in groups of 10. This helps in speedy processing without additional smearing that would occur otherwise. Depending upon the strength of the pulse, 1 to 4 folded profiles were obtained for each 9 minute data and were stored with appropriate time stamp.

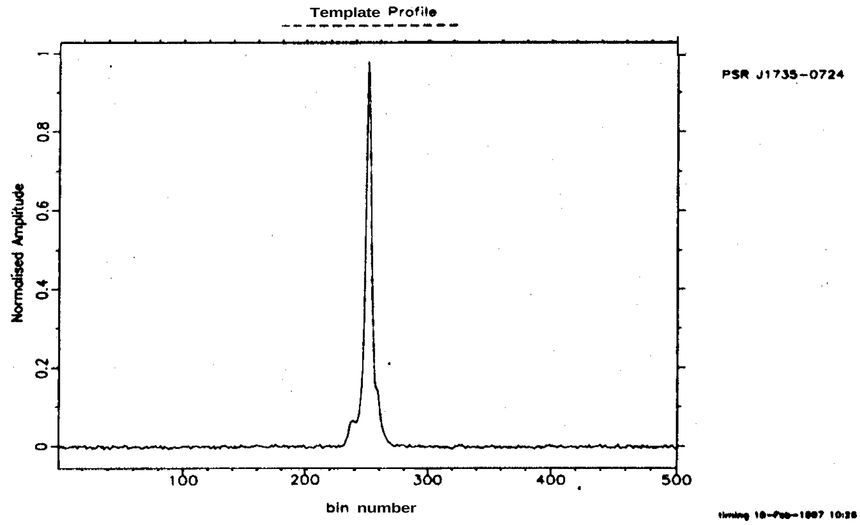

Figure 3.2: Template profile for PSR J17350724 produced from observations

The next step in the analysis of timing data is the estimation of pulse-arrival times at the observatory. This.step is usually accomplished by cross-correlation of the observed average profile with a template profile. Initially the template profile is generated by using gaussian or exponential function, or both convolved to an appropriate width, so **as** to resemble the observed pulse shape for a particular pulsar as far as possible. Soon a standard template can be obtained from observations themselves by averaging a large number of averaged profiles after suitable alignments. This gives us a high signal-to-noise ratio, noise-reduced template. An example of the template for the pulsar 517350724 is shown in fig(3.2).

Local or topocentric arrival time of an individual pulse refers to the arrival time of a unique point in the pulse (such as the centroid of the pulse) at the observatory. The delay $(\Delta t_{\text{profile}})$ corresponding to the maximum in the cross-correlation of the averaged profile with the template is measured. Estimation of the location of the maximum of the cross-correlation function was done using a 3-point parabolic interpolation (which seems to perform better compared to the commonly used 5-point or higher interpolation, see Deshpande & McCulloch 1993) around the peak of the function giving an improved estimate of the delay of the pulse profile with respect to the template profile. The rms 'measurement' uncertainty in the delay, σ_{delay} was estimated using the formula given by Downs & Reichley (1983)

$$\sigma_{\text{delay}} = \frac{(P\tau_b)^{1/2}}{\frac{S}{N}\left[\int_0^1 \left(\frac{dU}{d\phi}\right)^2 d\phi\right]^{1/2}} \tag{3.2}$$

where P is the pulse period, τ_b is the sampling interval, S/N is the signal-to-noise ratio of the pulse peak and U is the template function, ϕ is the phase across the profile. The integral in the denominator is a measure of the sharpness of the pulse. The measurement uncertainty in the delays estimated in our observations lies between 0.1-1 milliperiod.

The local arrival time is computed by combining the start time of the observation plus an integral number of periods close to the middle of the observation and the delay ($\Delta t_{\text{profile}}$), as

$$t_0 = T_{\text{start}} + \left[\text{int}\left(\frac{T}{2P}\right)\right] P + \Delta t_{\text{profile}} + \Delta t_{\text{ref}} \tag{3.3}$$

where t_0 is the local arrival time, T_{start} is the start time of the observation corrected for the drift in the Rb frequency standard, P is the period used for folding, T is the integration time and Δt_{ref} is the pulse offset in the template profile.

3.2 Estimation of Barycentric Arrival Time

The arrival time of pulses at the observatory is greatly modified by the effect of the Earth's rotation and revolution around the Sun. By referring the arrival times to an inertial reference frame, the Solar System Barycentre (SSB), these times are made independent of the Earth's motion. The following section describes the relevant corrections applied to the local arrival times (t_0).

We use the TEMPO package (Taylor & Weisberg 1989) for the estimation of barycentric arrival time. The barycentric arrival time t_b is given by

$$t_b = t_0 + \Delta t_{ob} - \Delta t_d + \Delta t_r - \Delta t_g \tag{3.4}$$

where t_0 is the arrival time at the observatory, Δt_{ob} is the light travel time from the observatory to barycentre, Δt_d is the dispersion delay at the Doppler-shifted frequency, At, is the relativistic correction of the Earth-bound clock due to the effects of a changing gravitational potential, and Δt_g is the Shapiro delay. The different terms are discussed below.

3.2.1 Time Standards and translation

The observation start time is measured in terms of the local time IST (Indian Standard Time). The normal convention is to quote the arrival times at the observatory in terms of universal titne standard. Hence IST is converted to UTC (Universal Co-ordinated time) by subtracting 5.5 hrs, which is the time difference between the UTC (Universal Time) and the IST. Universal Coordinated Time is translated to International Atomic Time (TAI) by adding an integral number of seconds known as 'leap seconds', this is because the UTC scale contains undesirable leap seconds in order to maintain consistency with mean solar time. Later TAI is translated to TDT (Terrestrial Dynamical Tirne) which has a constant offset of 32.184 s from TAI. Finally Earth proper time TDT is corrected to a uniformly

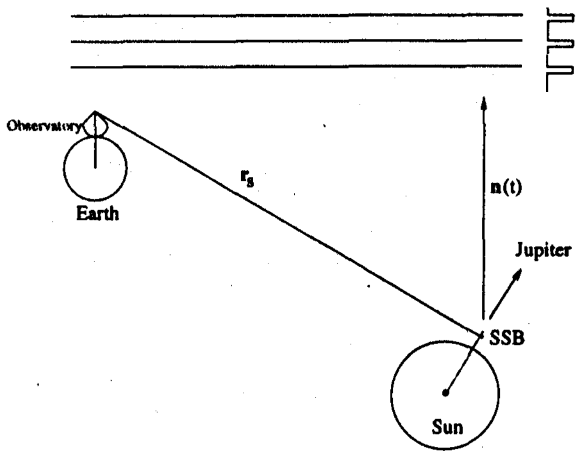

Figure 3.3: Space correction of telescope arrival time to the solar system barycentre

running coordinate time at the Solar System **Barycentre** (SSB), **Barycentric** Dynamical Time (TDB), by removing the gravitational **redshift** and time dilation effects around the Earth's orbit, explained in section (3.2.4). The inter-relation between the different times are summarized below.

$$\mathrm{UTC} = \mathrm{IST} - 5.5\ \mathbf{hrs} \quad (3.5)$$
$$\mathrm{TAI} = \mathrm{UTC} + \mathrm{leapseconds} \quad (3.6)$$
$$\mathrm{TDT} = \mathrm{TAI} + 32.184\ \mathrm{s} \quad (3.7)$$
$$\mathrm{TDB} = \mathrm{TDT} + 0.001658 \sin E \quad (3.8)$$

where E is the mean anomaly of the Earth's orbit. Improvements in the determination of the Earth's orbit **from** solar system observations, and possibly pulsar observations, will affect the TDT–TDB transformation. The stability of some pulsars may also lead to refinement of TAI.

3.2.2 Doppler delay

The first correction term in **eqn.(3.4)** is the Doppler correction term. The pulse-arrival-time difference between the observatory and SSB, given a pulsar direction, is

$$\Delta t_{ob} = \frac{\mathbf{r}_s \cdot \boldsymbol{n}}{c} \quad (3.9)$$

(Manchester & Taylor 1977) where r_s is the vector from the SSB to the observatory (fig 3.3), n is a unit vector in the assumed direction to the pulsar and c is the speed of light. The vector $\mathbf{r}_s/c$ was calculated **as** a combination of the three components: the vector from the observatory to centre of the Earth, ($\leq$ 22 ms); the Earth-centre to **Earth-**Moon **Barycentre** (EMB) vector ($\leq$ **20ms**); and the EMB to SSB vector (< 500s). The latter two steps are accomplished by interpolation from an ephemeris of the location of the moons and planets in the solar system. The Jet Propulsion Laboratories DE200 ephemeris (Standish 1982) was used to evaluate the location of the moons and the planets with the FK5 stellar refererice system at the epoch 52000.0. For all pulsars, the vector $\mathbf{n}$ was initially evaluated using the position given in the catalogue (Taylor, Manchester & Lyne 1993, latest version available from pulsar.princeton.edu ftp site). The position for all these pulsars had uncertainties of a few arcminutes, which we have tried to solve as a part of our timing analysis (section 3.3). An error of $0''.1$ in either the position of the pulsar or the orientation of the ephemeris co-ordinate system would introduce sinusoidal deviation of amplitude of $\sim 250\mu s$ in the computed arrival times.

3.2.3 Dispersive delay

The signal delay Δt_d due to the interstellar and interplanetary dispersion was calculated using the frequency $(\dot{\nu})$ at which the signal propagates through the interstellar medium rather than the observed frequency (which has been Doppler shifted by the Earth's motion). From equation(3.1), the time delay (in seconds) relative to a pseudo-infinite frequency is given by

$$\Delta t_d = \frac{DM}{2.410 \times 10^{-4} \nu^2} \tag{3.10}$$

where DM is the best available estimate of the pulsar dispersion measure in units of pc cm^{-3} and ν is in MHz.

3.2.4 Relativistic clock correction

The third correction term in equation(3.4), At,, accounts for the annual variation in the terrestrial clock rate relative to a clock at an infinite distance in a reference frame which is inertial with respect to the SSB. This variation results from the changing gravitational potential experienced by the terrestrial clock as the Earth moves around the Sun in an elliptical orbit. The relativistic clock correction was made using the approximation given by

$$\text{At}, = 1.66145 \times 10^{-3} \left[\left(1 - \frac{1}{8}e^2\right) \sin M_e + \frac{1}{2} e \sin 2M_e + \frac{3}{8} e^2 \sin 3M_e \right] \tag{3.11}$$

where e and M_e are the eccentricity and the mean anomaly of the Earth's orbit respectively. The first term introduces an annual sinusoidal variation of peak to peak amplitude 3.4ms, which is significant for timing observations. The higher order terms in equation(3.11) are normally neglected because of their low contribution of the order of $\sim \pm 20\mu s$, which is mainly due to the effects of the Moon and the planets.

3.2.5 Shapiro Delay

The last term, Δt_g is the relativistic delay, popularly known as Shapiro delay (Shapiro 1964), due to the curvature of the path of the pulsar signal as it traverses the gravitational field of the Sun. This delay is variable and it depends on the relative orientation of the Sun, the pulsar and the Earth. It reaches a maximum of $250\mu s$ when the line of sight is close to the Sun's limb (Backer & Hellings 1986).

3.3 Timing Models

Once a series of barycentric arrival times is obtained using equation(3.4), improved values of the pulsar parameters such as the period (P),period derivatives $(\dot{P})$ can be obtained. by a least-square fitting procedure. In order to obtain the pulsar spin-down parameters, a truncated Taylor series was used in the usual manner (Manchester & Taylor 1977)

$$\phi(t) = \phi_0 + \nu_0(t - t_0) + \dot{\nu}_0(t - t_0)^2 \tag{3.12}$$

where ν_0 is the rotation frequency $(= 1/P)$, $\dot{\nu}_0$ is the frequency derivative$(= -\dot{P}/P^2)$ at the reference epoch T_0. Using the above equation, the predicted phases, ϕ, at each observed epoch (barycentric arrival time) were calculated. The time differences between the expected and the observed pulse arrivals define the residuals (R). An error in assumed rotation frequency (ν_0) results in residuals that increase in time linearly, while an error in the frequency derivative results in a parabolic term in the residuals.

The observed residuals were modelled as

$$R = R_0 - \nu_0^{-1}(t - T_0)[\Delta\nu_0 + \Delta\dot{\nu}_0(t - T_0)] \tag{3.13}$$

in order to seek the best-fit values of the corrections; $\Delta\nu_0$ and $\Delta\dot{\nu}_0$ for the pulsar frequency and its first derivative respectively and in our case, $\dot{\nu}_0 = 0$ in the absence of its estimate to begin with. Least-square fitting to the residuals was performed initially for the data over short spans (a few tens of minutes) to obtain a better estimate of the period than was available from the catalogue and then the data spans for fitting extended to hours and then to days. This kind of bootstrapping is necessary to make sure that the pulse numbering remains valid, i.e. the residuals are free of integral phase cycle ambiguities.

Most of the pulsars in our list had more than a few arc minutes of uncertainties in their positions. Provided a data span of at least a year is available, reasonably accurate pulsar positions can be estimated from the arrival time data. From equation(3.4), an error in the assumed source position will result in a sinusoidal variation with a period of one year in the residuals. If second-order and higher terms are omitted, the terms representing offsets in right ascension and declination can be separated and included explicitly in the least squares of the residuals as (Manchester & Taylor 1977)

$$\begin{aligned} R \;=\; & R_0 - \nu_0^{-1}(t - t_0)\,[\Delta\nu_0 + \Delta\dot{\nu}_0(t - t_0)] + \\ & A\,[\Delta\alpha + \mu_\alpha(t - t_0)] + B\,[\Delta\delta + \mu_\delta(t - t_0)] \end{aligned} \tag{3.14}$$

where $\Delta\alpha$ and A6 are corrections to the assumed values of right ascension and declination, respectively and μ_α and μ_δ are the proper motions in right ascension and declination. If

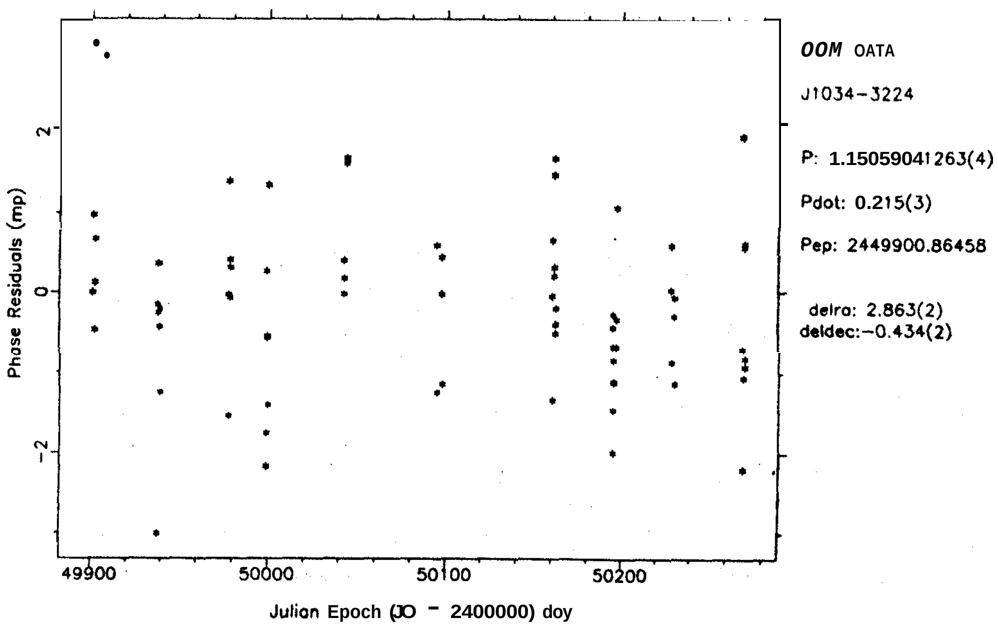

Figure 3.4: Post-fit timing residuals for the pulsar J1034-3224. The rms spread in the residuals is typically a few milliperiods as shown in this example. In the legend period is given in seconds, Pdot represents the period derivative (in 10^{-15} ss^{-1}) and Pep represents the reference epoch in Julian days for the period and the period derivative fitted. Delra and deldec are the positional errors (in arcminutes) fitted for.

---

several years of data are available, measurement of the proper motion of the pulsar is possible. The coefficients for the position-correction terms are

$$
\begin{aligned}
A &= \left(\frac{r_E}{c}\right) \cos\delta_E \cos\delta \sin(\alpha - \alpha_E) \\
B &= \left(\frac{r_E}{c}\right) [\cos\delta_E \sin\delta \cos(\alpha - \alpha_E) - \sin\delta_E \cos\delta]
\end{aligned}
\tag{3.15}
$$

where (a, δ) and (α_E, δ_E) are the co-ordinates of the pulsar and the earth, respectively with respect to the SSB and $\mathbf{r}_E$ is the distance from the earth to the barycentre.

Errors larger than an arcminute or so in the pulsar position could result in incorrect pulse numbering in spite of above mentioned bootstrapping. Hence, a combined fit for P, P and position is not possible when the uncertainty in each of these parameters is very large. So, in each case, an initial estimate of the position offset and P was obtained from the observed variations in the pulsar period as a function of epoch, where the periods over small epoch ranges were estimated by using a first-order polynomial fits to the preliminary phase residuals. Using these iriitial estimates, the phase residuals were reestimated and the bootstrapping method was applied on the phase residuals from which improved estimates of the positions, P and P were obtained. The improved estimates were found to be within the uncertainties of the initial estimates obtained from the period residuals (discussed in detail in **sec** 4.1). The post-fit phase residuals for one of the pulsars is shown in fig (3.4) to indicate the quality of our data and the goodness of the model fitted.

Summary of this chapter

Pulsar Timing is basically the measurement of the arrival time of the pulses. Its comparison with the expected arrival time is used to derive the pulsar rotational and positional parameters. This is done in a series of stages as follows:

- Determine the arrival time of the pulses in the observatory.
- **Translate** these arrival times to an inertial frame, Solar System **Barycentre,** by removing the effects of Earth's rotation, dispersive delays and other relativistic effects.
- Obtain the pulsar rotational and positional parameters by fitting a model for pulsar rotation to account for the **difference** between the observed and the expected arrival time of pulses.